Cell

NCoR1 Is a Conserved Physiological Modulator of Muscle Mass and Oxidative Function

Hiroyasu Yamamoto,[1] Evan G. Williams,[1] Laurent Mouchiroud,[1] Carles Cantó,[1] Weiwei Fan,[2] Michael Downes,[2] Christophe Héligon,[3] Grant D. Barish,[2] Béatrice Desvergne,[3] Ronald M. Evans,[2] Kristina Schoonjans,[1] and Johan Auwerx[1,*]

[1]Laboratory of Integrative and Systems Physiology (LISP), École Polytechnique Fédérale de Lausanne (EPFL), CH-1015 Lausanne, Switzerland

[2]Gene Expression Laboratory, Howard Hughes Medical Institute, The Salk Institute for Biological Studies, La Jolla, CA 92037, USA

[3]Centre for Integrative Genomics, University of Lausanne, CH-1015 Lausanne, Switzerland

*Correspondence: admin.auwerx@epfl.ch

DOI 10.1016/j.cell.2011.10.017

SUMMARY

Transcriptional coregulators control the activity of many transcription factors and are thought to have wide-ranging effects on gene expression patterns. We show here that muscle-specific loss of nuclear receptor corepressor 1 (NCoR1) in mice leads to enhanced exercise endurance due to an increase of both muscle mass and of mitochondrial number and activity. The activation of selected transcription factors that control muscle function, such as MEF2, PPARβ/δ, and ERRs, underpins these phenotypic alterations. NCoR1 levels are decreased in conditions that require fat oxidation, resetting transcriptional programs to boost oxidative metabolism. Knockdown of *gei-8*, the sole *C. elegans* NCoR homolog, also robustly increased muscle mitochondria and respiration, suggesting conservation of NCoR1 function. Collectively, our data suggest that NCoR1 plays an adaptive role in muscle physiology and that interference with NCoR1 action could be used to improve muscle function.

INTRODUCTION

Transcription factors are key mediators in homeostatic circuits, as they process environmental signals into transcriptional changes (Desvergne et al., 2006; Francis et al., 2003). Transcriptional coregulators have recently emerged as equally important modulators of such adaptive transcriptional responses. The fact that the activity of coactivators and corepressors is tightly regulated through the spatial and temporal control of their expression and activity levels opens another avenue to adapt transcription to environmental cues (Feige and Auwerx, 2007; Rosenfeld et al., 2006; Smith and O'Malley, 2004; Spiegelman and Heinrich, 2004). Interestingly, many of these coregulators do not operate in isolation but are part of large multiprotein complexes that integrate complex signaling pathways. The convergence of an elaborate coregulator network on the peroxisome proliferator-activated receptor (PPAR) coactivator α (PGC)-1α illustrates this principle well, as its activity depends on several other coregulators, including the steroid receptor coactivators, NR-interacting protein 1 or RIP140, CREB-binding protein, p300, protein arginine methyltransferase 1, general control of amino acid synthesis 5, and SIRT1 (Fernandez-Marcos and Auwerx, 2011; Handschin and Spiegelman, 2006).

The corepressor (NCoR1) and the silencing mediator for retinoid and thyroid hormone receptor (SMRT or NCoR2) are also acting as cofactor scaffolding platforms. NCoR1 and SMRT hardwire corepressor pathways that incorporate several deacetylases (including class I [HDAC3], class II [HDAC4, 5, 7, and 9], and class III [SIRT1] HDACs), transducin beta-like 1 (TBL1) and TBLR1, two highly related F box/WD40-containing factors, and the G protein pathway suppressor 2 (reviewed in Perissi et al., 2010). Because germline *NCoR1*$^{-/-}$ and *SMRT*$^{-/-}$ mice are embryonically lethal (Jepsen et al., 2000, 2007), information on the role of these proteins in adult physiology is limited. Studies of mice with mutations in the NR interaction domains (RIDs) 1 and 2 of SMRT (SMRTmRID), which solely disrupts its interaction with NRs, indicated that lethality of *SMRT*$^{-/-}$ mice is caused by non-NR transcription factors (Nofsinger et al., 2008). Work in 3T3-L1 cells in which NCoR1 or SMRT expression was reduced by RNA interference demonstrated that they repress adipogenesis by inhibiting PPARγ (Yu et al., 2005). In line with this, adipogenesis was enhanced in mouse embryonic fibroblasts (MEFs) from SMRTmRID mice (Nofsinger et al., 2008). Interestingly, SIRT1 is also part of the NCoR1/SMRT complex and contributes to the inhibition of PPARγ (Picard et al., 2004).

Contrary to adipose tissue, the function of NCoR1/SMRT in skeletal muscle has not yet been established. We here report the generation and characterization of muscle-specific *NCoR1*$^{-/-}$ (*NCoR1*$^{skm-/-}$) mice, which displayed a remarkable enhanced exercise capacity. This was the result of increased muscle mass and a muscle fiber type shift toward more oxidative fibers, coordinated by the induction of genes involved in mitochondrial biogenesis and function, ensuing from the activation

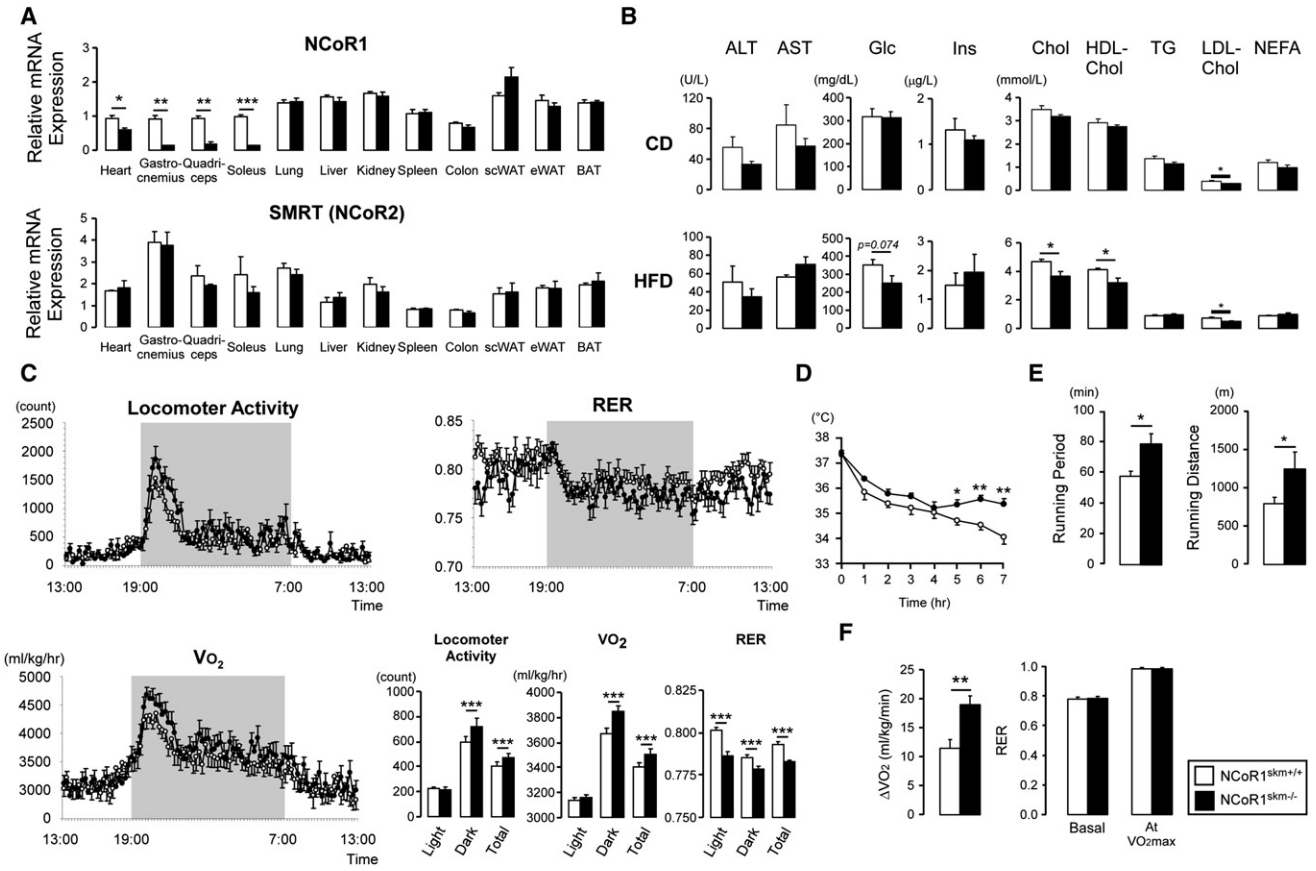

Figure 1. Validation and Metabolic Phenotypes of *NCoR1*$^{skm-/-}$ Mice

(A) mRNA levels of *NCoR1* and *Smrt* in different tissues were determined by qRT-PCR. Values were normalized to 36B4. n = 8–10/group.

(B) Biochemical analysis of the plasma from *NCoR1*$^{skm+/+}$ and $^{skm-/-}$ mice after 6 hr fasting (n = 8) either on chow diet (CD) (top) or HFD (bottom).

(C) Circadian activity, measured as the total locomotor activity, and energy expenditure were evaluated by the measurement of oxygen consumption (VO_2) and by the calculation of the respiratory exchange ratio (RER) over a 24 hr period after 12 weeks of HFD. The bar graphs represent the average for each group. n = 12.

(D) Body temperature was measured for 7 hr in mice exposed to 4°C after 18 weeks of HFD. n = 7–8.

(E and F) Exercise experiments, measuring running time and distance until exhaustion (endurance exercise) (E) and the increment of VO_{2max} during exercise and RER levels at basal and VO_{2max} condition (F) were performed after 14 and 17 weeks HFD.

Data are expressed as mean ± SEM. See also Figures S1–S3 and Tables S1–S3.

of PPARβ/δ, the estrogen-related receptors (ERRs), and myocyte-specific enhancer factor 2 (MEF2). Worms with a muscle-selective knockdown of *gei-8*, the sole *C. elegans* NCoR homolog, also had improved mitochondrial activity. These data combined with the specific reduction in the expression levels of NCoR1, but not SMRT, in situations of enhanced fat oxidation establish NCoR1 as a key physiological regulator of muscle mass and function.

RESULTS

NCoR1$^{skm-/-}$ Mice Have Increased Muscle Mass

Given the embryonic lethality of germline *NCoR1*$^{-/-}$ mice (Jepsen et al., 2000) (Table S1 available online), we generated a floxed NCoR1 mouse line in which exon 11 of the *NCoR1* gene (Hörlein et al., 1995) was flanked with LoxP sites, priming it for subsequent deletion using the Cre-LoxP system. These mice, bearing floxed *NCoR1* L2 alleles, were then bred with a skeletal muscle (skm)-specific Cre driver (human α-skeletal actin promoter) (Miniou et al., 1999) to yield *NCoR1*$^{skm-/-}$ and *NCoR1*$^{skm+/+}$ mice (Figure S1). As expected, *NCoR1* mRNA expression was significantly decreased in soleus, gastrocnemius, and quadriceps and modestly reduced in the heart muscle of *NCoR1*$^{skm-/-}$ mice, but not altered in other tissues (Figure 1A). No compensatory induction of the related corepressor SMRT/NCoR2 (Chen and Evans, 1995) was observed (Figure 1A). We also tried to determine NCoR1 protein levels in muscle but failed to detect the endogenous protein with the currently available NCoR1 antibodies.

NCoR1$^{skm-/-}$ mice were indistinguishable from *NCoR1*$^{skm+/+}$ mice upon visual inspection, and no gross organ anomalies were revealed upon autopsy. The relative mass of the soleus muscle was higher, whereas the mass of the gastrocnemius showed a trend toward an increase, which did not reach statistical significance (Figures S2A and S2B). The soleus was also more intensely red, and there were larger sections with reddish

color in the gastrocnemius in *NCoR1*$^{skm-/-}$ mice (Figure S2C). Body weight evolution and food intake of male *NCoR1*$^{skm-/-}$ and *NCoR1*$^{skm+/+}$ mice after weaning were comparable both on chow diet (CD) and on high-fat diet (HFD) (Figure S2A and data not shown). On CD, carbohydrate and lipid profiles were similar except for LDL cholesterol, which was reduced in *NCoR1*$^{skm-/-}$ mice (Figure 1B). In addition to the lower LDL cholesterol on CD, total and HDL cholesterol levels were also reduced in *NCoR1*$^{skm-/-}$ mice on HFD (Figure 1B). Furthermore, glucose edged down ($p = 0.074$) in the wake of similar insulin levels on HFD. The slightly reduced area under the curve in intraperitoneal glucose tolerance test (IPGTT; Figure S2D) and the delayed recovery from hypoglycemia during intraperitoneal insulin tolerance test (IPITT; Figure S2E) in mutant mice on HFD may suggest a discrete improvement in insulin sensitivity but without a clear impact on glucose tolerance.

Enhanced Exercise Performance in *NCoR1*$^{skm-/-}$ Mice

We next evaluated energy expenditure by indirect calorimetry and actiometry in CD- and HFD-fed mice (Figures 1C and S2F). Total locomotor activity was significantly higher in *NCoR1*$^{skm-/-}$ mice. Consistent with this, O_2 consumption (VO_2) was increased under both CD and HFD. Interestingly, the *NCoR1*$^{skm-/-}$ mice displayed a marked decrease in the respiratory exchange ratio (RER) on a HFD (Figure 1C), indicating an enhanced use of fat as a main energy source. *NCoR1*$^{skm-/-}$ mice were also more cold tolerant, as they maintained their body temperature better when exposed to 4°C (Figure 1D).

Exercise performance was strikingly improved in *NCoR1*$^{skm-/-}$ mice (Figures 1E, 1F, and S3A–S3D). In endurance exercises, *NCoR1*$^{skm-/-}$ mice ran for a significantly longer time and distance before exhaustion (Figures 1E, S3A, and S3B). The increase of the VO_2 values (ΔVO_2) during exercise and the maximal ability to utilize oxygen during exercise (VO_{2max}), which critically determines the endurance performance of skeletal muscle, was slightly higher in *NCoR1*$^{skm-/-}$ mice on both CD (Figure S3D and data not shown) and HFD (Figure 1F). Despite the moderate reduction in *NCoR1* mRNA levels in cardiac muscle of *NCoR1*$^{skm-/-}$ mice, heart rate, blood pressure, cardiac morphology, and function were not changed (Figures S3E–S3G and Table S2).

NCoR1$^{skm-/-}$ Muscle Demonstrates Increased Oxidative Capacity

The enhanced exercise capacity, associated with the increase in overall muscle mass and change in muscle appearance, led us to examine muscle morphology. Upon staining muscles with hematoxylin/eosin or toluidine blue, not only was the diameter of single muscle fibers larger, but also the connective tissue between muscle bundles was less abundant in *NCoR1*$^{skm-/-}$ mice (Figures 2A, 2B, and S4A). The increased number of intensely stained fibers upon succinate dehydrogenase (SDH) and cytochrome oxidase (COX) (Figures 2C and 2D) staining further testified to increased mitochondrial activity in the *NCoR1*$^{skm-/-}$ gastrocnemius. Two mitochondrial DNA markers, cyclooxygenase 2 (*Cox2*) and 16S ribosomal RNA, normalized by genomic DNA markers (uncoupling protein 2 [*Ucp2*] and hexokinase 2 [*Hk2*]) were both significantly higher in *NCoR1*$^{skm-/-}$ muscle, indicative of increased mitochondrial content (Figure 3B). This observation was also underscored by electron microscopy, which revealed more abundant and larger mitochondria with normal structure (Figure 3A). Immunohistochemical analysis of the myosin heavy-chain (MyHC) isoforms (Schiaffino et al., 1989) demonstrated a decreased number of the more glycolytic MyHC2b fibers, with a concomitant increase in the number of more oxidative MyHC2x and 2a fibers in the *NCoR1*$^{skm-/-}$ gastrocnemius (Figure 3C). This observation was consolidated by analysis of MyHC isoform mRNAs, which indicated an increased expression of the mRNAs of *MyHC2x* and *2a* (more oxidative fibers) compared to that of *MyHC2b* (more glycolytic) in both *NCoR1*$^{skm-/-}$ gastrocnemius and quadriceps (Figure 3D). In quadriceps, but not gastrocnemius, the expression of *MyHC1* mRNA was also increased. Finally, staining of platelet-endothelial cell adhesion molecule (PECAM)-1, an endothelial cell marker of angiogenesis and tissue vascularization that contributes to enhanced myocellular aerobic capacity, also increased in *NCoR1*$^{skm-/-}$ muscle (Figure S5C).

The Control of Muscle Mitochondria by NCoR1 Is Conserved in *C. elegans*

To investigate whether the effects of NCoR1 deficiency are evolutionary conserved, we took advantage of the power of *C. elegans* genetics. A protein blast search indicated that *GEX-interacting protein family member 8* (*gei-8*) is the only putative NCoR1 homolog in the *C. elegans* genome. Further analysis showed that the total amino acid sequence of *gei-8* is 43% homologous to mouse NCoR1 and contained conserved SANT (switching-defective protein 3 [Swi3], adaptor 2 [Ada2], nuclear receptor corepressor [N-CoR], transcription factor [TF] IIIB) domains (34% identical/77% similar for SANT1; 20% identical/57% similar for SANT2) (Figure 3E). Other important functional domains (repressor domain [RD] and nuclear receptor interaction domain [ID]) were also conserved (Figure 3E). Upon the robust *gei-8* knockdown in worms expressing a mitochondrial GFP reporter driven by the muscle-specific *myo-3* promoter, a striking enlargement of the mitochondria was observed in body wall muscle (Figure 3F). This result is not due to an indirect effect on transcriptional activity through the *myo-3* promoter because no increase in GFP expression is observed with another strain carrying the $_p$myo-3::GFP reporter (Figure S4B). We also measured O_2 consumption in NR350 transgenic worms fed with *gei-8* dsRNA. NR350 worms lack *rde-1*, an essential component of the RNAi machinery encoding a member of the PIWI/STING/Argonaute family, in all tissues except the body wall muscle in which the wild-type *rde-1* gene has been rescued using the *hlh-1* promoter (Durieux et al., 2011). Consistent with the effects observed in the mouse, also the muscle-specific knockdown of *gei-8* enhanced O_2 consumption in these NR350 worms (Figure 3G), suggesting that the function of *gei-8* to control mitochondrial metabolism is conserved through evolution.

NCoR1 Negatively Correlates with Key Mitochondrial and Myogenic Genes

After establishing these striking mitochondrial effects of NCoR1 in mice and worms, we exploited a complementary systems

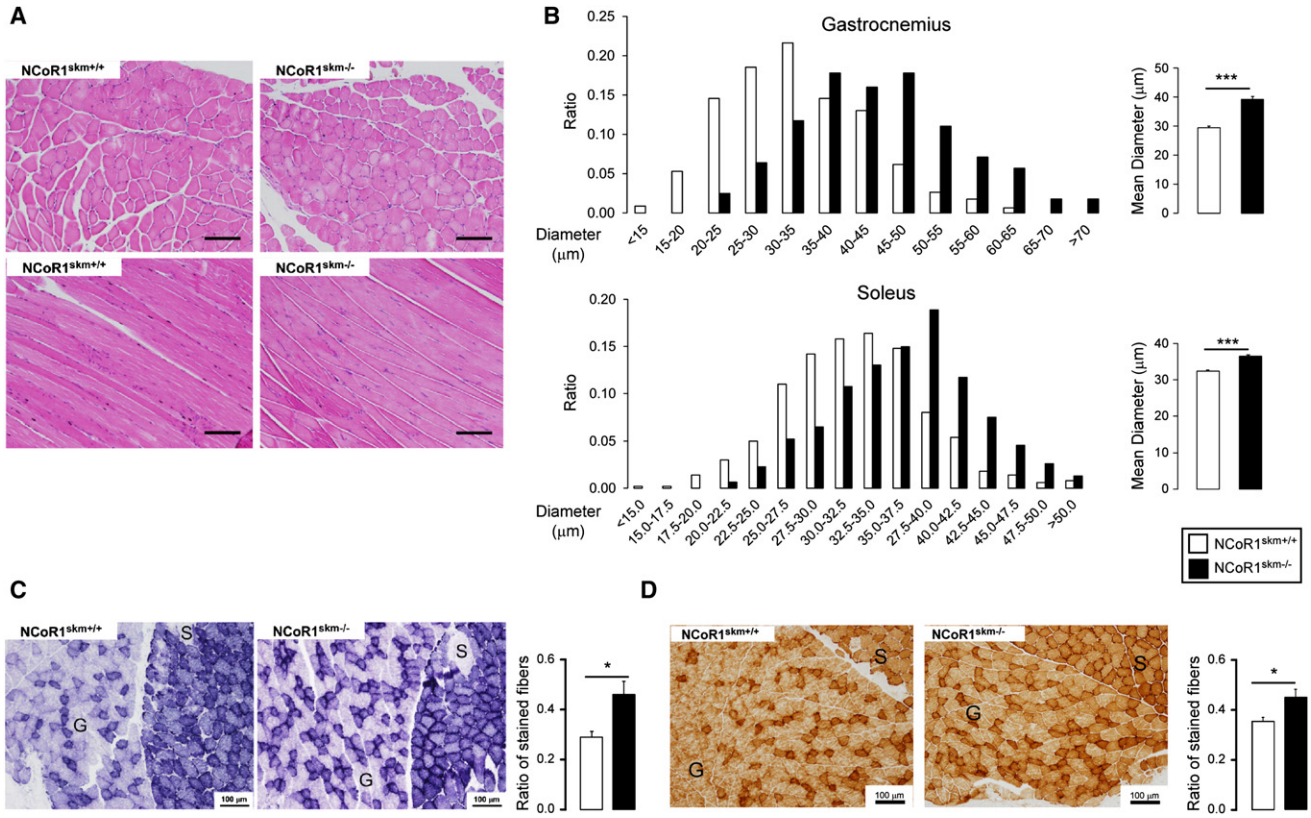

Figure 2. Histological Analyses of the Muscles of Control and *NCoR1*$^{skm-/-}$ Mice

(A) Histological analysis of gastrocnemius sections stained with hematoxylin and eosin.

(B) Distribution and mean diameter of muscle fibers in gastrocnemius and soleus.

(C and D) Histological analysis of gastrocnemius and soleus sections by succinate dehydrogenase (C) and cytochrome C oxidase staining (D). S, soleus; G, gastrocnemius. The ratio of the stained fibers is indicated in the graph.

Data are expressed as mean ± SEM. See also Figure S4.

genetics approach to evaluate *NCoR1*s molecular coexpression partners in the mouse (Argmann et al., 2005; Houtkooper et al., 2010). Expression of *NCoR1* in two panels of genetically heterogeneous mice, made by intercrossing C57BL/6 with C3H/HeJ (the B×H F2 cross) or C57BL/6 with DBA/2J (the B×D genetic reference population) mice, varied ± 1.5-fold between cases in both lung and muscle (Figure 4A). A large number of transcripts covaried significantly with *NCoR1* in the different mice lines belonging either to the B×H cross or B×D strains. Most distinctively, only a fraction of these covariates were negative, which was against the dogma expected for a corepressor such as *NCoR1s* (Tables S4 and S5). In skeletal muscle from the B×H cross (n = 124 females), strong covariates of *NCoR1* include *Mef2d*, myoglobin (*Mb*), muscle creatine kinase (*Mck*), and glucose transporter type 4 (*Glut4*) (van Nas et al., 2010). A similar analysis of lung tissue from the B×D cross (n = 51 strains) includes genes such as cytochrome c (*Cycs*), citrate synthase (*Cs*), pyruvate dehydrogenase kinase 4 (*Pdk4*), uncoupling protein 3 (*Ucp3*), vascular endothelial growth factor b (*Vegfb*), and long-chain acyl-CoA dehydrogenase (*Lcad*) (Alberts et al., 2011) (Figure 4B and Tables S4 and S5). This analysis significantly extends the number of *NCoR1* targets and covariates, with several of them being consistent with increased mass and mitochondrial biogenesis observed in *NCoR1*$^{skm-/-}$ muscle.

This initial set of *NCoR1* covariates (Figure 4B) was then included together with other potential candidates for qRT-PCR analysis in mixed fiber muscle, including the gastrocnemius and quadriceps (Figures 4C and S5A and data not shown). Whereas the mRNAs of most relevant NRs were unchanged, mRNA levels of PGC-1α and β (*Ppargc1a* and *1b*) increased. Several genes involved in mitochondrial function, including those encoding for proteins involved in TCA cycle and oxidative phosphorylation (*Cs*, cytochrome c oxidase subunit IV [*CoxIV*], *Pdk4*), uncoupling (*Ucp2* and *Ucp3*), fatty acid uptake, and metabolism (*Cd36* and *Lcad*), were robustly induced in *NCoR1*$^{skm-/-}$ muscle. In addition, mRNA levels of *Vegfb* and its receptor *Flt1*, which regulates *trans*-endothelial fatty acid transport (Hagberg et al., 2010), were also induced. Interestingly, the expression of hypoxia-inducible factor (*Hif*) 1α and of its targets, glucose transporter 1 (*Glut1*), fibroblast growth factor (*Fgf*), and *Fgf*-receptor 2 (*Fgfr2*), were unchanged (Figure S5A), whereas all three *Vegfa* isoforms, i.e., *Vegfa*-121, -165, and -189, were induced in *NCoR1*$^{-/-}$ quadriceps, gastrocnemius,

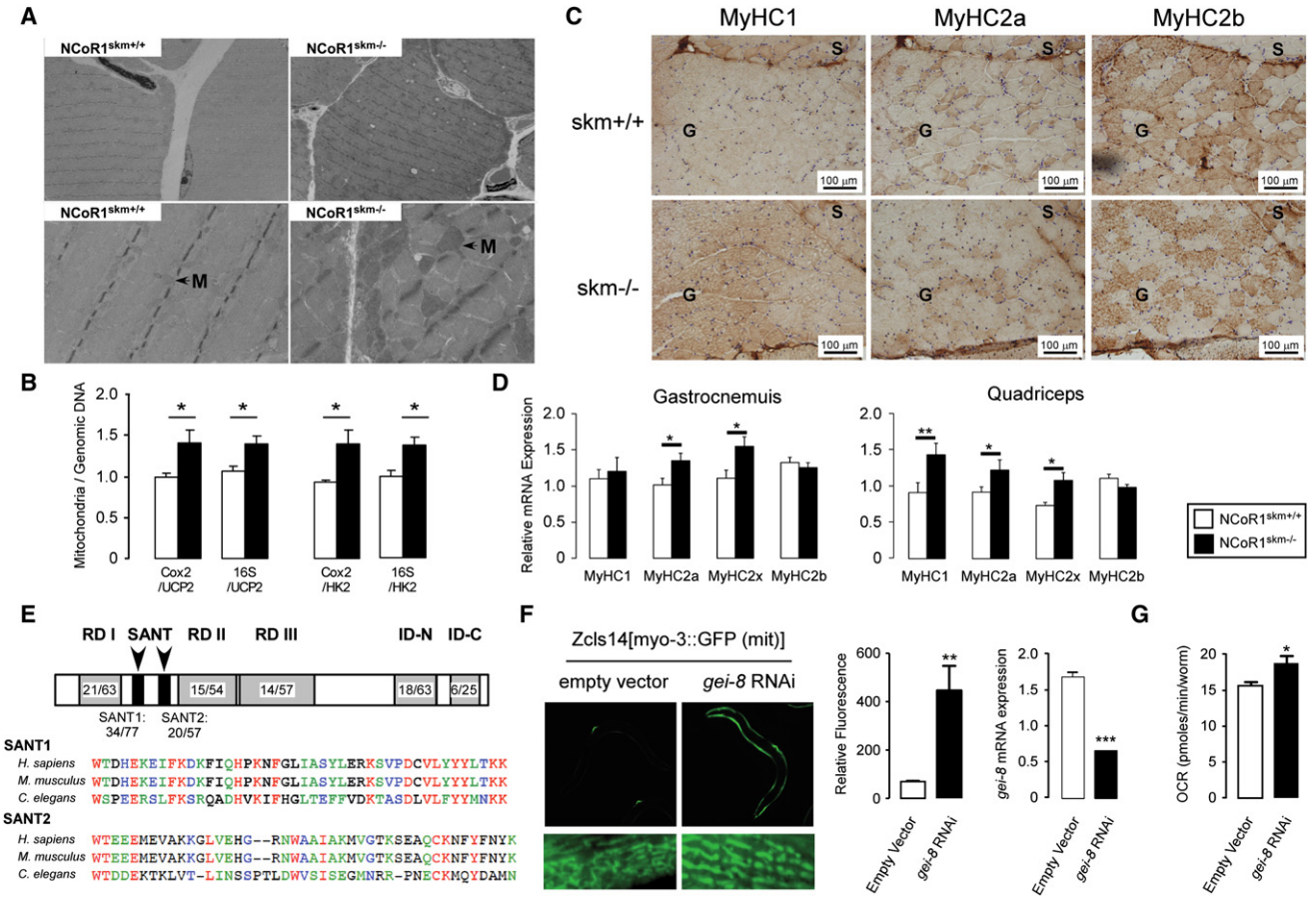

Figure 3. Histological Analyses of the Muscles of Mice and *C. elegans*

(A) Transmission electron microscopy of nonoxidative fibers of *NCoR1*$^{skm+/+}$ and $^{skm-/-}$ gastrocnemius. M, mitochondria.

(B) Relative mitochondrial DNA content (*Cox2* or *16S*) in gastrocnemius was measured and normalized by genomic DNA content (*Ucp2* and *Hk*). n = 6.

(C) Representative MyHC1, 2a, and 2b immunohistochemical detection on serial sections of the soleus and gastrocnemius.

(D) Subtypes of MyHCs in gastrocnemius and quadriceps were analyzed by qRT-PCR in *NCoR1*$^{skm+/+}$ and $^{skm-/-}$ mice. n = 6.

(E) Identity/similarity (%) in the sequences of *gei-8* with mammalian NCoR1. Multiple alignments of SANT domains of NCoR1 homologs. Color identifies similarity.

(F) Representative pictures of the effects of RNAi-mediated knockdown of *gei-8* on mitochondrial morphology and number in a *C. elegans* strain carrying a mitochondrial GFP reporter driven by the muscle-specific *myo-3* promoter (left). Quantification of the mitochondrial induction by fluorescence upon *gei-8* knockdown (middle) and of the efficacy of the RNAi-mediated *gei-8* knockdown by qRT-PCR analysis (right).

(G) Muscle-specific RNAi inhibition of *gei-8* enhances respiration in *C. elegans*.

Data are expressed as mean ± SEM. See also Figure S4 and Tables S2 and S3.

and soleus (Figures 4C and 5B). Together with this increase in *Vegfa*, both *Angpt2* and *Pdgfb* mRNA levels were induced (Figure 4C), suggesting that myocellular aerobic capacity is facilitated by an HIF1α-independent angiogenic pathway in *NCoR1*$^{skm-/-}$ mice (Arany et al., 2008).

Enhanced PPARβ/δ and/or ERR Function in *NCoR1*$^{skm-/-}$ Muscle

Several genes whose expression is changed in the absence of NCoR1 are PPARβ/δ and/or ERR targets (Figure 4). Because the expression of PPARβ/δ and/or ERR was unchanged in *NCoR1*$^{skm-/-}$ mice (Figure S5A), a direct effect of NCoR1 on the expression of these targets through the activation of these NRs was expected. As cases in point to demonstrate the recruitment of NCoR1 to these genes, we selected the mouse *Ucp3* and *Pdk4* promoters, which contain three PPAR responsive elements (PPREs) (Figure 5A) and extended NR half-sites (NR1/2), known to bind members of the ERR subfamily (Figure 5E) (Zhang et al., 2006), respectively. We first used NIH 3T3 cells in which an epitope-tagged version of NCoR1 (NCoR1-FLAG) was expressed. The two PPREs adjacent to the *Ucp3* transcription start site recruited NCoR1 more efficiently, compared to two control sequences in the *Gapdh* and *Ucp3* promoter that lack PPREs (Figure 5B, left). Likewise, NCoR1 bound avidly to the mouse *Pdk4* promoter NR1/2 site in transfected NIH 3T3 cells (Figure 5F, left). Although there is a two nucleotide difference in NR1/2 site of the human *Pdk4* promoter (Figure 5E), NCoR1 and ERRα were also recruited to this site in human HEK293 cells (Figure 5H).

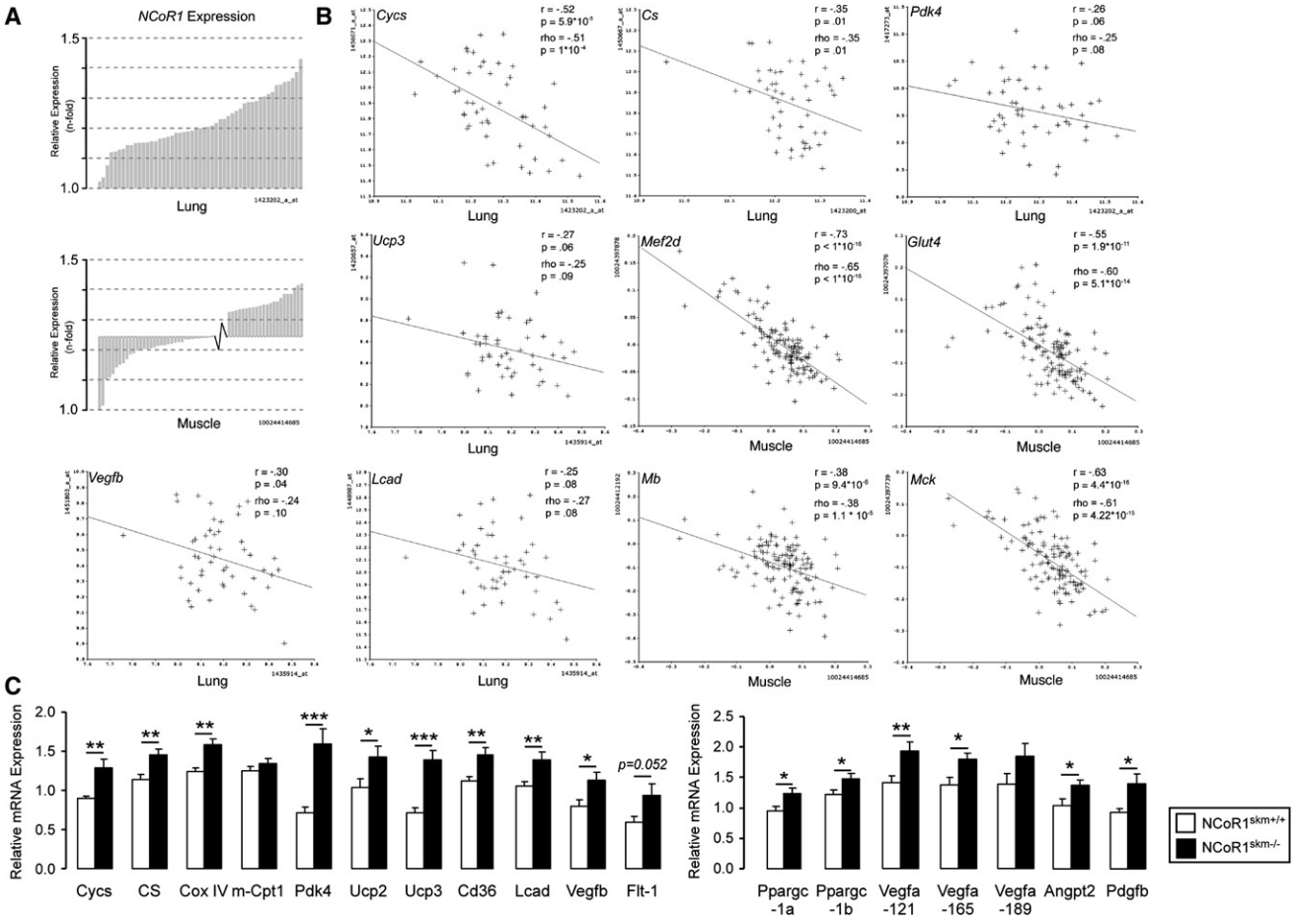

Figure 4. Identification of *NcoR1*-Correlated Genes

(A) Expression of *NCoR1* mRNA in lung tissue of the different B×D strains (top) and in muscle tissue from an F2 intercross between C57BL/6J and C3H/HeJ (bottom). Natural expression variation across the animals is ~1.5-fold in each tissue.

(B) Pearson's *r* and Spearman's rank correlation coefficient, *rho*, were calculated with corresponding p values for the mRNA covariation between *NCoR1* and genes involved in oxidative phosphorylation (*Cycs*, *Cs*, and *Pdk4*), mitochondrial uncoupling (*Ucp3*), fatty acid metabolism (*Lcad*), angiogenesis (*Vegfb*), glucose uptake (*Glut4*), and myogenesis (*Mef2d*, *Mb*, and *Mck*). The tissue from which data were generated is indicated.

(C) Gene expression analysis by qRT-PCR in $NCoR1^{skm+/+}$ and $^{skm-/-}$ gastrocnemius. n = 10.

Data are expressed as mean ± SEM. See also Figures S5 and S6 and Tables S3–S5.

We then used a highly specific NCoR1 antibody, which we recently generated (G.D.B. and R.M.E., unpublished data), for ChIP experiments in C2C12 myotubes. Confirming our data in NIH 3T3 cells that express NCoR1-FLAG, endogenous NCoR1 occupied the same *Ucp3* PPREs (Figure 5B, right). The recruitment of NCoR1 to the *Ucp3* promoter was robustly inhibited by the addition of the selective PPARβ/δ ligand GW501516. Likewise, endogenous NCoR1 was readily detected on the NR1/2 in the *Pdk4* promoter in C2C12 myotubes (Figure 5F, right).

Subsequently, we explored whether *NCoR1* gene deletion in $NCoR1^{L2/L2}$ MEFs by means of adenoviral Cre recombination, or *NCoR1* gene knockdown in C2C12 myotubes infected by an NCoR1 shRNA adenovirus, modulates histone H4 acetylation on the *Ucp3* and *Pdk4* promoters. Consistent with NCoR1 binding to these promoters in NIH 3T3 cells and C2C12 myotubes (Figures 5B and 5F), NCoR1 deletion or silencing induced H4 acetylation of both target promoters in MEFs and C2C12 cells, indicating chromatin opening (Figures 5C and 5G).

To further consolidate these observations, we analyzed whether NCoR1 interacts directly with PPARβ/δ or ERRα, using nuclear extracts of HEK293 cells, transfected with tagged versions of NCoR1, PPARβ/δ, or ERRα. Although a specific association between NCoR1 and PPARβ/δ was evident in these co-IP experiments (Figure 5D, lane 8), we failed to detect a similar interaction between ERRα and NCoR1 (data not shown).

MEF2 Is Hyperacetylated and Activated in the Absence of NCoR1

The increased muscle mass observed in $NCoR1^{skm-/-}$ mice indicated that the absence of *NCoR1* not only induced oxidative metabolism, but also stimulated myogenesis. In line with this,

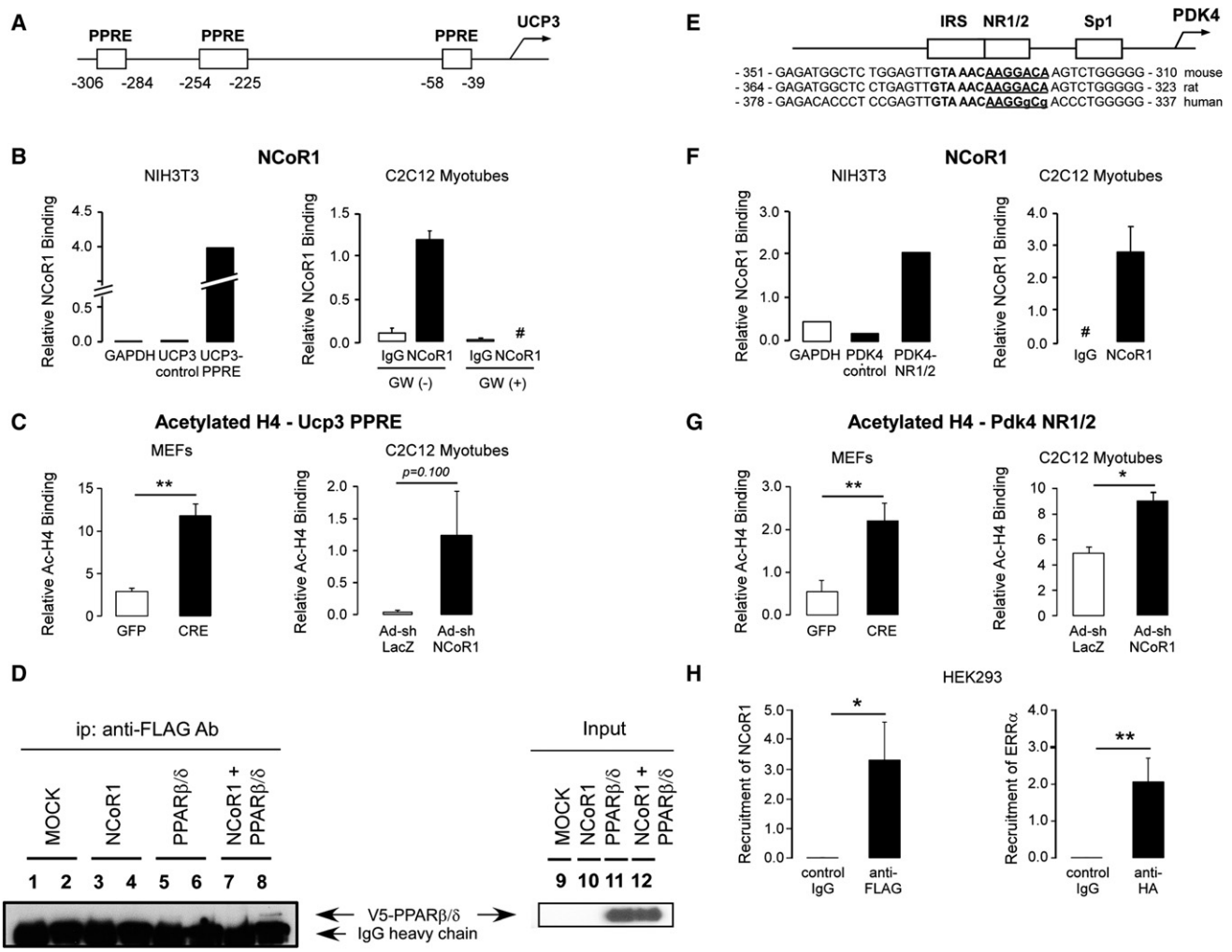

Figure 5. Increased PPARβ/δ and ERR Activity in *NCoR1*$^{skm-/-}$ Muscle

(A, B, E, F, and H) NCoR1 recruitment to the PPREs on mouse *Ucp3* promoter (B) and to the ERR-RE on human (H) and mouse (F) *Pdk4* promoter determined by ChIP in NIH 3T3 cells transfected with an NCoR1-FLAG vector or in C2C12 myotubes. A schematic of the promoters of the *Ucp3* (A) and *Pdk4* (E) genes and the sequence alignment of the mouse, rat, and human *Pdk4* promoter is also shown to highlight the conservation of the NR1/2 (or ERR-RE) (E). Boxes indicate putative PPREs in the *Ucp3* and the NR1/2, IRS, and Sp1 in the *Pdk4* promoter. ChIP experiments for the *Ucp3* promoter were performed in C2C12 myotubes both before and 6 hr after addition of a PPARβ/δ agonist (100 nM GW501516). #, not detected. ChIP experiments in HEK293 cells transfected with FLAG-NCoR1 and HA-ERRα vector (H).

(C and G) Binding of acetylated histone 4 (H4) to the PPREs on the *Ucp3* and to the NR1/2 on the *Pdk4* promoters in ChIP assays, using either immortalized *NCoR1*$^{L2/L2}$ MEFs, infected with an adenovirus either expressing GFP or Cre recombinase, or C2C12 myotubes infected with the Ad-shNCoR1 virus. Representative data are shown from three experiments.

(D) Interaction between PPARβ/δ and NCoR1 determined by in vitro co-IP experiments from HEK293 cells in which NCoR1-FLAG and/or V5-PPARβ/δ are expressed. IP was performed with control IgG (lanes 1, 3, 5, and 7) or anti-FLAG antibody (lanes 2, 4, 6, and 8), and the immunoblot was developed with an anti-V5 antibody. PPARβ/δ coimmunoprecipitated by the anti-FLAG antibody is indicated by an arrow. Input samples are shown in lanes 9–12.

Data are expressed as mean ± SEM. See also Figure S6.

mRNA levels of two markers of myogenesis, *Mb* and *Mck*, were increased in *NCoR1*$^{skm-/-}$ quadriceps (Figure 6A). Among several myogenic regulatory factors, only the expression of two *Mef2* family members, i.e., *Mef2c* and *Mef2d*, negatively correlated with *NCoR1* expression in our systems genetics analysis (Figures 4 and S6A). The selective induction of *Mef2c* and *Mef2d* mRNA was furthermore confirmed by qRT-PCR of *NCoR1*$^{skm-/-}$ gastrocnemius and quadriceps, whereas no changes were found in *MyoD*, *Myf5*, and *myogenin* mRNA (Figures 6A and S6E and data not shown).

The activity of MEF2 family members is not only controlled by their expression levels, but is also modulated by their acetylation status. MEF2 is acetylated and activated by p300, whereas it is deacetylated by HDAC3 and HDAC4, which are part of the NCoR1 corepressor complex (Ma et al., 2005; Nebbioso et al., 2009). Because the expression of the *Mef2d* isoform is most

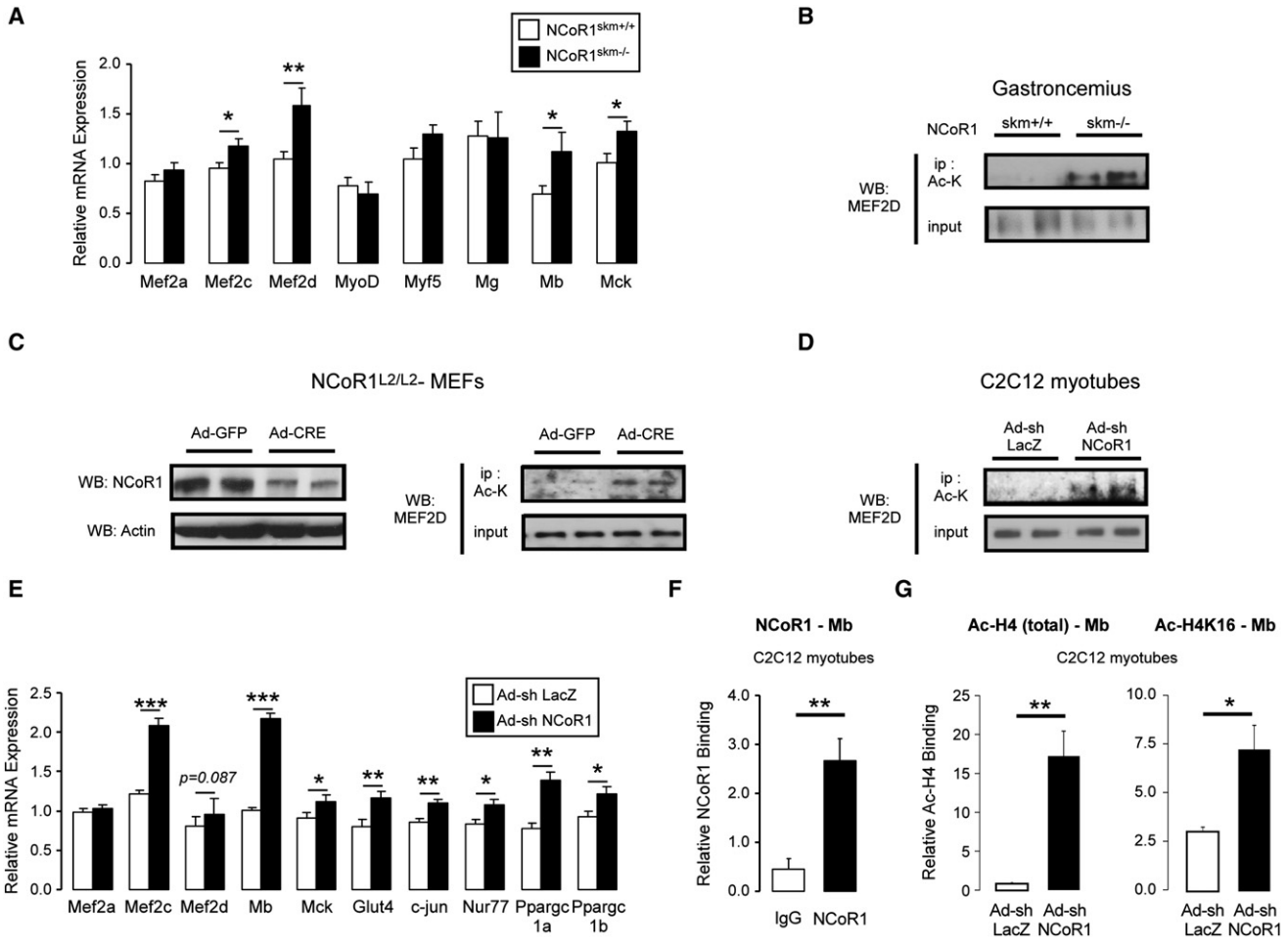

Figure 6. Enhanced MEF2 Activity in *NCoR1*$^{skm-/-}$ Muscle

(A) Gene expression of myogenesis-related genes was measured by qRT-PCR in *NCoR1*$^{skm+/+}$ and $^{skm-/-}$ quadriceps. n = 10.

(B–D) Acetylation levels of MEF2D were determined by western blot after immunoprecipitation with an Ac-Lys Ab from gastrocnemius (B), from *NCoR1*$^{L2/L2}$ MEFs infected with Ad-GFP or Ad-Cre recombinase (C, right), and from C2C12 myotubes infected with Ad-shLacZ or Ad-shNCoR1 (D). MEF2D expression in total protein extracts was shown in the bottom panels. The expression of NCoR1 and actin in *NCoR1*$^{L2/L2}$ MEFs was also shown (C, left).

(E) MEF2 target mRNAs determined by qRT-PCR in C2C12 myotubes infected with either Ad-shLacZ or Ad-shNCoR1. n = 6.

(F) NCoR1 recruitment to the MEF2 site of the mouse *Mb* promoter determined by ChIP in C2C12 myotubes.

(G) Binding of either global acetylated histone 4 (H4) or H4 acetylated on K16 (H4K16) to the MEF2 site of the *Mb* gene was evaluated by ChIP from C2C12 myotubes infected as in (E).

Data are expressed as mean ± SEM. See also Figure S6 and Table S3.

prominently correlated with *NCoR1* expression, we investigated MEF2D acetylation in gastrocnemius and found that its acetylation levels were enhanced in *NCoR1*$^{skm-/-}$ mice (Figures 6A and 6B).

We then compared the acetylation of MEF2D in floxed *NCoR1*$^{L2/L2}$ MEFs, infected with an adenovirus expressing either GFP as control or Cre-recombinase to reduce NCoR1 protein expression (Figure 6C, left). Whereas MEF2D protein levels were stable in *NCoR1*$^{-/-}$ MEFs, perhaps due to the more acute nature of the deletion, MEF2D was robustly hyperacetylated when NCoR1 levels were attenuated (Figure 6C, right). Likewise, a slight but consistent MEF2D hyperacetylation was observed in C2C12 myotubes infected with Ad-shNCoR1 to knock down *NCoR1* expression (Figures 6D and S6B–S6D), further underscoring the importance of MEF2D deacetylation by the NCoR1 complex.

Given the induction of MEF2D expression and its hyperacetylation and consistent with our systems genetics analysis (Figure 4B), mRNA levels of the MEF2 targets, *Mb* and *Mck*, were robustly induced in *NCoR1*$^{skm-/-}$ gastrocnemius (Figure 6A). Silencing of *NCoR1* in C2C12 myotubes also resulted in a similar induction of several MEF2 target genes, including *Mb*, *Mck*, *Glut4*, *c-Jun*, *Nur77*, *PGC-1α*, and *PGC-1β* (Figures 6E and S6B–S6D). In line with these data, endogenous NCoR1 was readily detected on MEF2-binding sites on these target promoters in C2C12 myotubes, as illustrated for the *Mb*

promoter (Figure 6F). The induction of these MEF2 targets by NCoR1 knockdown was furthermore accompanied by H4K16 and global H4 hyperacetylation on their promoters (e.g., *Mb*, *Glut4*, and *Mck*) (Figures 6G and S6F).

NCoR1 Levels Are Regulated in Response to Physiological Stimuli

We next investigated whether NCoR1 function could be altered by different physiological stimuli in vitro and in vivo. One hour after stimulation of 293T cells with 1 μM insulin, higher amounts of endogenous NCoR1 (Figure 7A) or transfected FLAG-NCoR1 (Figure S7A) were detected in nuclei, as evidenced by immunofluorescence and subcellular fractionation (Figures 7A–7C).

At the transcriptional level, *NCoR1* mRNA changed in response to different concentrations of glucose in the culture media (Figures 7D and 7E). Growing MEFs in low glucose decreased NCoR1 mRNA (Figure 7D) and protein (Figure 7E) levels, concomitant with the induction of its target genes (*Pdk4*, *Vgefb*, *Mef2d*, etc.). Similar results, i.e., decreased mRNA levels of *NCoR1* associated with increased expression of its targets (*Pdk4*, *Ucp2*, *Ucp3*, *Vegfb*, *Mb*, *Mck*, and *Glut4*) were also obtained in glucose-deprived C2C12 myotubes (Figure S7B). Interestingly, the reduction of glucose decreased mRNA levels of *NCoR1*, but not those of *SMRT* (Figure 7F). The tight dose-dependent correlation between *NCoR1* expression and glucose levels in the culture medium (Figures 7E and 7F) suggested the possibility that NCoR1 could block the oxidation of lipid substrates when glucose was available. We therefore evaluated NCoR1 mRNA and protein in MEFs cultured in different fatty acid concentrations (Figure 7H and 7I). The addition of oleic acid (OA) to the medium to force fatty acid oxidation also decreased *NCoR1* levels, independently of the glucose concentration (Figure 7H). These effects seemed again specific to *NCoR1*, as only a small difference in *SMRT* mRNA levels was observed with OA in the absence of glucose (data not shown). Together, these data indicate that settings that favor fatty acid oxidation (i.e., low glucose, low insulin, and high fatty acid) are all associated with a reduction of NCoR1.

We then tested whether different conditions that enhance fatty acid oxidation also modulate *NCoR1* mRNA levels in the muscle in vivo. This was indeed the case, as muscle *NCoR1*, but not *SMRT*, mRNA levels decreased after exercise (3 hr after a resistance run), high-fat feeding (20 weeks of high fat feeding), fasting (after a 16 hr fast), and aging (6-month-old versus 2-year-old mice) (Figure 7J and data not shown). Interestingly, the reduction in *NCoR1* mRNA levels matches well with the potentiation of lipid oxidation after exercise (Kiens and Richter, 1998; Pilegaard et al., 2000), high-fat feeding (Watanabe et al., 2006), and fasting (Storlien et al., 2004) and in aged mice (Houtkooper et al., 2011). Also in epididymal white adipose tissue, HFD feeding reduced specifically *NCoR1*, and not *SMRT*, mRNA (Figure S7C). Unlike for the muscle, where we were unable to detect NCoR1 with the available antibodies, NCoR1 protein levels almost disappeared from epididymal fat upon HFD (Figure S7D). Altogether, these data led us to suggest that NCoR1 is a negative transcriptional regulator of fatty acid oxidation and that a reduction of NCoR1 enables the muscle (and adipose tissue) to deal with lipid substrates more efficiently.

DISCUSSION

The increased muscle mass, associated with a strikingly improved exercise capacity, is the most prominent phenotypic outcome of the muscle-specific *NCoR1* gene deletion. The enhanced exercise capacity is associated with a reprogramming of glycolytic to more oxidative muscle fibers and a corresponding stimulation of oxidative mitochondrial metabolism, indicative of an improved intrinsic quality of the muscles. The increased muscle quantity and oxidative profile in $NCoR1^{skm-/-}$ mice also contribute to the slight improvement in metabolic parameters after high-fat feeding and to the cold resistance subsequent to shivering thermogenesis (Cantó and Auwerx, 2009).

Combined, these properties suggest that NCoR1 acts as a master modulator of mitochondrial metabolism in the muscle, a hypothesis bolstered by the fact that the inhibition of the single worm NCoR homolog, *gei-8*, also robustly boosts muscle oxidative mitochondrial metabolism in *C. elegans*. The evolutionary conservation of the structure and function of this corepressor makes it tempting to speculate that NCoR may have evolved to facilitate metabolic adaptation of the mitochondria to energy availability, as has been described for other cofactors as SIRT1 (Cantó and Auwerx, 2009).

As to how the absence of NCoR1 in the muscle achieves these remarkable effects, it is important to recall that NCoR1 docks histone deacetylases, such as HDAC3 (Alenghat et al., 2008) and SIRT1 (Picard et al., 2004). The use of mice with a point mutation in the NCoR1 deacetylase activation domain, incapacitating its interaction with HDAC3, indicated that this interaction is a nodal point in epigenetic regulation (Alenghat et al., 2008; Feng et al., 2011). The physiological alterations in the $NCoR1^{skm-/-}$ muscle together with the study of the expression correlates of *NCoR1* suggested that, rather than the generalized transcriptional activation expected upon ablation of a corepressor platform protein, only a small set of transcriptional pathways was selectively affected.

Several transcription factors control muscle differentiation and development, including MyoD, myogenin, Myf5, Myf6, and MEF2 (Black and Olson, 1998; McKinsey et al., 2001, 2002; Potthoff and Olson, 2007). MEF2 especially caught our attention, as only its expression negatively correlated with *NCoR1* (Figures 4B and S6) and was induced in $NCoR1^{skm-/-}$ muscle (Figure 6A). MEF2 is key for muscle development and also participates in muscle stress response and remodeling in adulthood, such as occurs during muscle fiber type switch (Potthoff and Olson, 2007; Zhang et al., 2002). MEF2 activity is not only controlled at the level of its expression, but also by a wide range of intracellular signaling pathways and interacting coregulator molecules (reviewed by Potthoff and Olson, 2007). The histone acetyltransferases, p300/CBP, bind, acetylate, and activate MEF2 (Ma et al., 2005; McKinsey et al., 2001), whereas class I (HDAC3 [Grégoire et al., 2007]), class II (HDAC4, 5, 7, and 9 [Haberland et al., 2007; McKinsey et al., 2001]), and class III HDACs (SIRT1 [Zhao et al., 2005]) all are reported to interact with MEF2 and prevent the activation of its target genes (McKinsey et al., 2001). The absence of NCoR1 would hence favor the acetylation and activation of MEF2. The hyperacetylation of MEF2D and histone 4 in *NCoR1*-deficient MEFs, C2C12 myotubes, and muscles, which

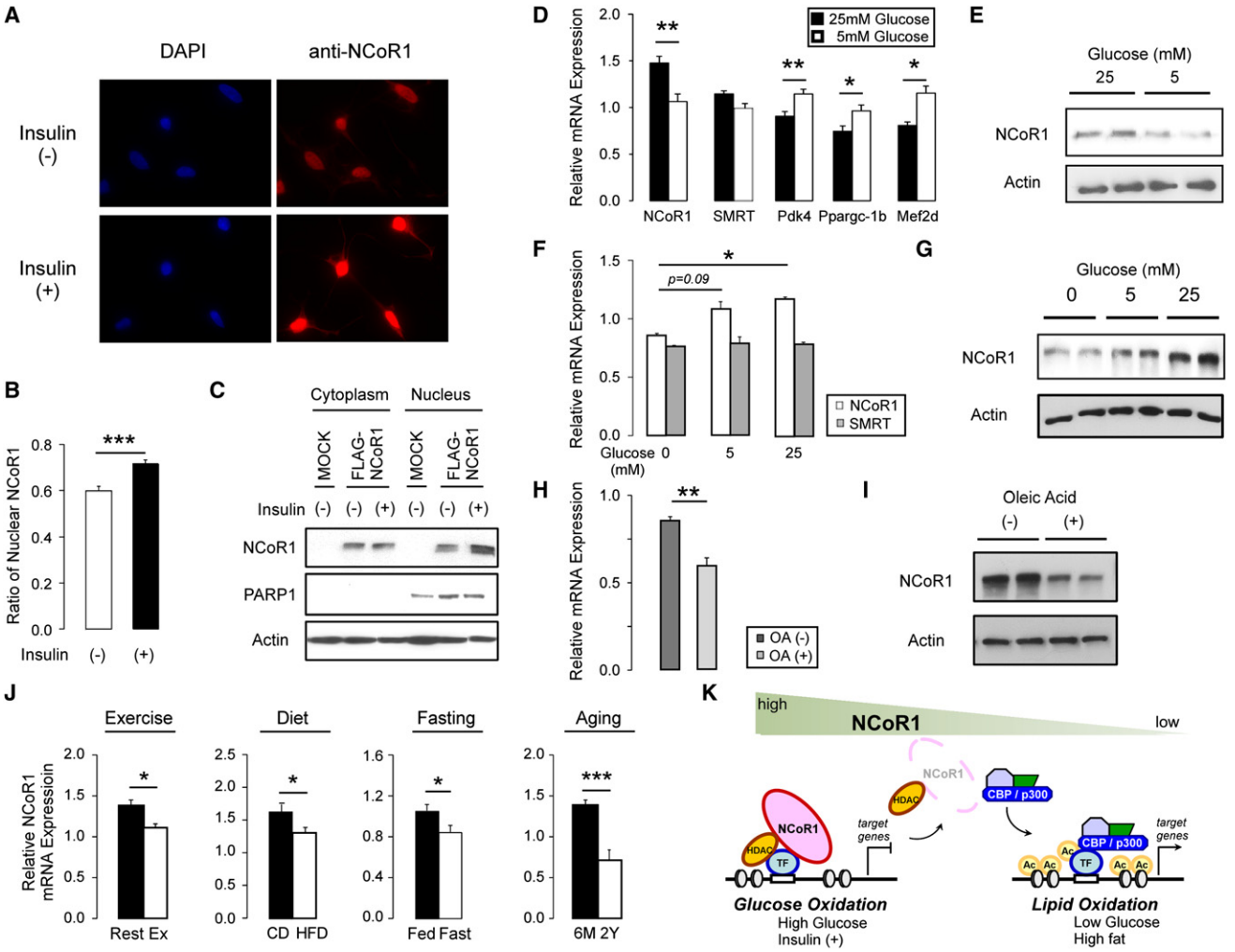

Figure 7. Localization and Expression of NCoR1 in Physiological Conditions

(A–C) Localization of NCoR1 protein was determined either by immunofluorescence and quantified (A and B) or by western blot (C). 293T cells grown without (−) or with (+) 1 μM insulin for 1 hr were stained by DAPI or anti-NCoR1 (A). Quantification of nuclear NCoR1 is shown in (B). Nuclear and cytosolic fractions were separated from FLAG-NCoR1-transfected 293T cells after a 1 hr stimulation without (−) or with 1 μM insulin (+), and protein levels were determined by western blotting (C).

(D) mRNA levels of *NCoRs* and its target genes determined by qRT-PCR in MEFs cultured for 24 hr in 5 or 25 mM glucose. n = 6.

(E) NCoR1 protein was determined by western blotting from MEFs cultured for 24 hr in 5 or 25 mM glucose.

(F) *NCoR1* and *SMRT* mRNA were determined in MEFs cultured for 48 hr in 0, 5, and 25 mM glucose.

(G) NCoR1 protein was determined by western blotting from MEFs cultured for 24 hr in 0, 5, or 25 mM glucose.

(H) *NCoR1* mRNA expression in MEFs grown for 48 hr in 0 mM glucose with or without 0.03 mM oleic acid. n = 4.

(I) NCoR1 protein determined by western blotting from MEFs cultured as indicated in (G).

(J) *NCoR1* mRNA measured by qRT-PCR in muscles of resting mice or 3 hr after an endurance run (14 weeks old; n = 5), in mice that were fed for 20 weeks either HFD or CD (28 weeks old; n = 8), in mice that were fasted or fed for 16 hr (14 weeks old; n = 10), and in 6-month-old or 2-year-old mice (n = 10).

(K) Model schematizing how different levels of NCoR1 control transcription of muscle genes by controlling the activity of transcription factors (TFs), i.e., PPARβ/δ, ERR, and MEF2.

Data are expressed as mean ± SEM. See also Figure S7 and Table S3.

translates into the induction of MEF2 targets and the gain of muscle mass in *NCoR1*$^{skm-/-}$ mice, is fully in line with this idea (Figure 6).

The increased expression of genes related to fatty acid catabolism and mitochondrial respiration underlies the oxidative mitochondrial changes observed in the *NCoR1*$^{skm-/-}$ mice. In the muscle, the expression of these gene sets is tightly controlled by NRs belonging to the PPAR and ERR families (Alaynick, 2008). PPARβ/δ, the predominant PPAR isoform in oxidative fibers, regulates oxidative capacity and enhances slow fiber-type function, resulting in improved exercise capacity and metabolic protection (Luquet et al., 2003; Tanaka et al., 2003; Wang et al., 2004). Among the ERRs, mainly ERRα and ERRγ seem to be involved in the coordination of muscle energy homeostasis

(reviewed in Giguère, 2008; Villena and Kralli, 2008). In line with this, a genome-wide location analysis of ERRα and ERRγ identified binding sites in genes of a large number of mitochondrial proteins (Dufour et al., 2007), and studies in mouse models show that they coordinate many aspects of muscle oxidative metabolism, including endurance capacity (Giguère, 2008; Narkar et al., 2011; Villena and Kralli, 2008). Several features of the *NCoR1*$^{skm-/-}$ mice are suggestive of the activation of PPARβ/δ and ERR. The demonstration that NCoR1 is recruited to the PPREs in the *Ucp3* and the NR1/2 in *Pdk4* promoters and that histone 4 is hyperacetylated on these promoters when NCoR1 is absent suggests that coactivators now activate the transcription of these genes in a fashion unopposed by the NCoR1 corepressor platform (Figure 7K). Given that PGC-1α is a key coactivator of PPARβ/δ and ERR transcriptional programs (reviewed in Handschin and Spiegelman, 2006]), it is no surprise that several phenotypic features, ranging from similarities in gene expression patterns over the induction of mitochondrial oxidative metabolism and exercise capacity to HIF1α-independent angiogenesis, are shared between mice that lack NCoR1 or that overexpress PGC-1α (Arany et al., 2008; Lin et al., 2002).

NCoR1 action is tightly regulated by various physiological challenges, and this is achieved through at least two different mechanisms. First, nuclear levels of NCoR1 are regulated. Our results show how insulin, which stimulates glucose oxidation at the expense of fatty acid oxidation, increases NCoR1 levels in the nucleus, enabling it to subsequently repress lipid oxidation genes. Interestingly, this effect of insulin on nuclear NCoR1 accumulation is consistent with the positive effect of mTORC1 on nuclear NCoR1 accumulation, recently reported in hepatocytes (Sengupta et al., 2010). The second mechanism involves the modulation of NCoR1 expression. Exposing cells to media with low glucose and/or high fatty acid levels reduces specifically *NCoR1* (but not *SMRT*) mRNA and protein levels, ultimately derepressing genes that control oxidative lipid metabolism. Likewise, endurance exercise, fasting, high-fat feeding, and aging—conditions paired with increased fat oxidation—also are characterized by attenuated muscle *NCoR1* mRNA expression. Although we are unable to detect NCoR1 protein in the muscle with the currently available antibodies, our data in adipose tissue unequivocally show that the specific reduction in *NCoR1* mRNA observed in that tissue after HFD is matched with a spectacular drop in NCoR1 protein. If the reduced *NCoR1* mRNA levels in muscle also translate to corresponding changes in NCoR1 protein, they will prime the muscle for mitochondrial oxidation. These selective effects of NCoR1 to repress muscle fatty acid oxidation hence suggest that changes in NCoR1 levels adapt transcriptional outcomes to physiological energy needs (Figure 7K).

In conclusion, we demonstrated here that NCoR is an evolutionary conserved negative regulator of both muscle mass and mitochondrial oxidative metabolism in nematode and mammals. In the mouse, NCoR1 achieves these effects through controlling a rather selected set of functional pathways, which are governed by MEF2, PPARβ/δ, and the ERRs. The *NCoR1*$^{skm-/-}$ muscle phenotype furthermore mirrors many features of the stimulation of PGC-1α, a coactivator, whose action is less constrained by the absence of the NCoR1 corepressor scaffold. Our work also provides evidence that NCoR1 expression is regulated in a dynamic fashion and, as such, could play a role similar to PGC-1α in transcriptional adaptation to physiological challenges. Moreover, pharmacological inhibition of NCoR1 and/or its interaction with deacetylases may be a viable approach to improve muscle mass and oxidative metabolism. The fact that the inhibition of HDACs increases muscle cell size supports this concept (Iezzi et al., 2004). It is also tempting to speculate that the beneficial effects of the inhibition of mTORC1 and insulin signaling on health and life span may, in part, rely on the attenuation of NCoR1 activity and the subsequent induction of oxidative metabolism in the muscle (reviewed in Houtkooper et al., 2010).

EXPERIMENTAL PROCEDURES

Animal Studies

NCoR1 floxed (*NCoR1*$^{L2/L2}$), *NCoR1*$^{skm+/+}$, and $^{skm-/-}$ mice were generated at the Mouse Clinical Institute (Strasbourg, France) and phenotyped (Champy et al., 2004, 2008) according to standard procedures that are described in detail in the Extended Experimental Procedures. *C. elegans* strains, RNAi feeding experiments, and GFP expression analysis are described in the Extended Experimental Procedures. *C. elegans* O_2 consumption was measured in 200 2-day-old worms using a Seahorse XF24, as described in the Extended Experimental Procedures.

Histological and EM Analyses

Staining of muscles with hematoxylin and eosin, immunohistochemical and EM analysis, and analysis of enzymatic activity of SDH and COX were carried out as described (Lagouge et al., 2006).

mRNA Analysis and Identification of NCoR1-Correlated Genes

The mRNA expression levels were measured in cells and tissues using qRT-PCR (Lagouge et al., 2006) The GeneNetwork program (http://www.genenetwork.org) was used to generate a broad range of NCoR1-correlated genes that may contribute to the phenotype of *NCoR1*$^{skm-/-}$ mice. Skeletal muscle mRNA expression was analyzed using 124 females from a classic F2 intercross between C57BL/6J and C3H/HeJ (UCLA BHHBF2 Muscle; van Nas et al., 2010; GEO GSE12795). *NCoR1* (10024414685, 3′ UTR) was compared across all transcripts to find muscle covariates. Lung mRNA in a recombinant inbred intercross between C57BL/6J and DBA/2J was analyzed across 51 strains (HZI BXD Lung M430v2 [Apr08] RMA; Alberts et al., 2011]. Four *NCoR1* probe sets from this microarray were analyzed (1423200_at, 3′UTR; 1435914_at, 3′UTR; 1423202_a_at, exonic and 3′UTR; 1423201_at, exonic). For all probe sets, the top correlates were calculated (Tables S4 and S5). Strong or interesting correlates were selected for validation by qRT-PCR.

Cell Culture, Adenoviral Infections, ChIP, co-IP, and Western Blot Experiments

Experimental details are provided in the Extended Experimental Procedures.

Statistical Analyses

Statistical analyses were performed with a Student's t test for independent samples. Data are expressed as mean ± SEM, and p values smaller than 0.05 were considered as statistically significant. *$p < 0.05$; **$p < 0.01$; ***$p < 0.001$.

SUPPLEMENTAL INFORMATION

Supplemental Information includes Extended Experimental Procedures, seven figures, and five tables and can be found with this article online at doi:10.1016/j.cell.2011.10.017.

ACKNOWLEDGMENTS

We acknowledge M. Lazar (University of Pennsylvania, Philadelphia), A. Kralli (Scripps Research Institute, San Diego), J.-S. Annicotte and L. Fajas (Institut de Génétique Moléculaire de Montpellier, France), A. Lusis (University of California, Los Angeles), K. Schughart (Helmholtz Zentrum, Hannover, Germany), R. Williams (University of Tennessee Health Science Center, Memphis), and the Caenorhabditis Genetics Center (CGC) for generous sharing of research reagents and data. We thank N. Messadeq (Institut Clinique de la Souris, Strasbourg, France) for EM analysis and the Center for PhenoGenomics (CPG) at the EPFL for help with mouse phenotyping. This work was supported by the École Polytechnique Fédérale de Lausanne, Swiss National Science Foundation, NIH (DK059820 to J.A., DK062434 to R.M.E., 1K08HL092298 to G.D.B., HD027183 to R.M.E., and DK057978 to R.M.E.), the EU ideas program (ERC-2008-AdG-23118), the Helmsley Charitable Trust, the Glenn Foundation, and the Howard Hughes Medical Institute (HHMI). H.Y. was supported by an FRM fellowship. R.M.E. is an Investigator of the HHMI and the March of Dimes Chair in Molecular and Developmental Biology. J.A. is the Nestle Chair in Energy Metabolism. We thank the members of the Auwerx lab and R. Williams for discussions.

Received: January 31, 2011
Revised: August 9, 2011
Accepted: October 6, 2011
Published: November 10, 2011

REFERENCES

Alaynick, W.A. (2008). Nuclear receptors, mitochondria and lipid metabolism. Mitochondrion *8*, 329–337.

Alberts, R., Lu, L., Williams, R.W., and Schughart, K. (2011). Genome-wide analysis of the mouse lung transcriptome reveals novel molecular gene interaction networks and cell-specific expression signatures. Respir. Res. *12*, 61.

Alenghat, T., Meyers, K., Mullican, S.E., Leitner, K., Adeniji-Adele, A., Avila, J., Bućan, M., Ahima, R.S., Kaestner, K.H., and Lazar, M.A. (2008). Nuclear receptor corepressor and histone deacetylase 3 govern circadian metabolic physiology. Nature *456*, 997–1000.

Arany, Z., Foo, S.Y., Ma, Y., Ruas, J.L., Bommi-Reddy, A., Girnun, G., Cooper, M., Laznik, D., Chinsomboon, J., Rangwala, S.M., et al. (2008). HIF-independent regulation of VEGF and angiogenesis by the transcriptional coactivator PGC-1alpha. Nature *451*, 1008–1012.

Argmann, C.A., Chambon, P., and Auwerx, J. (2005). Mouse phenogenomics: the fast track to "systems metabolism". Cell Metab. *2*, 349–360.

Black, B.L., and Olson, E.N. (1998). Transcriptional control of muscle development by myocyte enhancer factor-2 (MEF2) proteins. Annu. Rev. Cell Dev. Biol. *14*, 167–196.

Cantó, C., and Auwerx, J. (2009). PGC-1alpha, SIRT1 and AMPK, an energy sensing network that controls energy expenditure. Curr. Opin. Lipidol. *20*, 98–105.

Champy, M.F., Selloum, M., Piard, L., Zeitler, V., Caradec, C., Chambon, P., and Auwerx, J. (2004). Mouse functional genomics requires standardization of mouse handling and housing conditions. Mamm. Genome *15*, 768–783.

Champy, M.F., Selloum, M., Zeitler, V., Caradec, C., Jung, B., Rousseau, S., Pouilly, L., Sorg, T., and Auwerx, J. (2008). Genetic background determines metabolic phenotypes in the mouse. Mamm. Genome *19*, 318–331.

Chen, J.D., and Evans, R.M. (1995). A transcriptional co-repressor that interacts with nuclear hormone receptors. Nature *377*, 454–457.

Desvergne, B., Michalik, L., and Wahli, W. (2006). Transcriptional regulation of metabolism. Physiol. Rev. *86*, 465–514.

Dufour, C.R., Wilson, B.J., Huss, J.M., Kelly, D.P., Alaynick, W.A., Downes, M., Evans, R.M., Blanchette, M., and Giguère, V. (2007). Genome-wide orchestration of cardiac functions by the orphan nuclear receptors ERRalpha and gamma. Cell Metab. *5*, 345–356.

Durieux, J., Wolff, S., and Dillin, A. (2011). The cell-non-autonomous nature of electron transport chain-mediated longevity. Cell *144*, 79–91.

Feige, J.N., and Auwerx, J. (2007). Transcriptional coregulators in the control of energy homeostasis. Trends Cell Biol. *17*, 292–301.

Feng, D., Liu, T., Sun, Z., Bugge, A., Mullican, S.E., Alenghat, T., Liu, X.S., and Lazar, M.A. (2011). A circadian rhythm orchestrated by histone deacetylase 3 controls hepatic lipid metabolism. Science *331*, 1315–1319.

Fernandez-Marcos, P.J., and Auwerx, J. (2011). Regulation of PGC-1α, a nodal regulator of mitochondrial biogenesis. Am. J. Clin. Nutr. *93*, 884S–90.

Francis, G.A., Fayard, E., Picard, F., and Auwerx, J. (2003). Nuclear receptors and the control of metabolism. Annu. Rev. Physiol. *65*, 261–311.

Giguère, V. (2008). Transcriptional control of energy homeostasis by the estrogen-related receptors. Endocr. Rev. *29*, 677–696.

Grégoire, S., Xiao, L., Nie, J., Zhang, X., Xu, M., Li, J., Wong, J., Seto, E., and Yang, X.J. (2007). Histone deacetylase 3 interacts with and deacetylates myocyte enhancer factor 2. Mol. Cell. Biol. *27*, 1280–1295.

Haberland, M., Arnold, M.A., McAnally, J., Phan, D., Kim, Y., and Olson, E.N. (2007). Regulation of HDAC9 gene expression by MEF2 establishes a negative-feedback loop in the transcriptional circuitry of muscle differentiation. Mol. Cell. Biol. *27*, 518–525.

Hagberg, C.E., Falkevall, A., Wang, X., Larsson, E., Huusko, J., Nilsson, I., van Meeteren, L.A., Samen, E., Lu, L., Vanwildemeersch, M., et al. (2010). Vascular endothelial growth factor B controls endothelial fatty acid uptake. Nature *464*, 917–921.

Handschin, C., and Spiegelman, B.M. (2006). Peroxisome proliferator-activated receptor gamma coactivator 1 coactivators, energy homeostasis, and metabolism. Endocr. Rev. *27*, 728–735.

Hörlein, A.J., Näär, A.M., Heinzel, T., Torchia, J., Gloss, B., Kurokawa, R., Ryan, A., Kamei, Y., Söderström, M., Glass, C.K., et al. (1995). Ligand-independent repression by the thyroid hormone receptor mediated by a nuclear receptor co-repressor. Nature *377*, 397–404.

Houtkooper, R.H., Williams, R.W., and Auwerx, J. (2010). Metabolic networks of longevity. Cell *142*, 9–14.

Houtkooper, R.H., Argmann, C., Houten, S.M., Cantó, C., Jeninga, E.H., Andreux, P.A., Thomas, C., Doenlen, R., Schoonjans, K., and Auwerx, J. (2011). The metabolic footprint of aging in mice. Sci. Rep. Published online October 31, 2011. 10.1038/srep00134.

Iezzi, S., Di Padova, M., Serra, C., Caretti, G., Simone, C., Maklan, E., Minetti, G., Zhao, P., Hoffman, E.P., Puri, P.L., and Sartorelli, V. (2004). Deacetylase inhibitors increase muscle cell size by promoting myoblast recruitment and fusion through induction of follistatin. Dev. Cell *6*, 673–684.

Jepsen, K., Hermanson, O., Onami, T.M., Gleiberman, A.S., Lunyak, V., McEvilly, R.J., Kurokawa, R., Kumar, V., Liu, F., Seto, E., et al. (2000). Combinatorial roles of the nuclear receptor corepressor in transcription and development. Cell *102*, 753–763.

Jepsen, K., Solum, D., Zhou, T., McEvilly, R.J., Kim, H.J., Glass, C.K., Hermanson, O., and Rosenfeld, M.G. (2007). SMRT-mediated repression of an H3K27 demethylase in progression from neural stem cell to neuron. Nature *450*, 415–419.

Kiens, B., and Richter, E.A. (1998). Utilization of skeletal muscle triacylglycerol during postexercise recovery in humans. Am. J. Physiol. *275*, E332–E337.

Lagouge, M., Argmann, C., Gerhart-Hines, Z., Meziane, H., Lerin, C., Daussin, F., Messadeq, N., Milne, J., Lambert, P., Elliott, P., et al. (2006). Resveratrol improves mitochondrial function and protects against metabolic disease by activating SIRT1 and PGC-1alpha. Cell *127*, 1109–1122.

Lin, J., Wu, H., Tarr, P.T., Zhang, C.Y., Wu, Z., Boss, O., Michael, L.F., Puigserver, P., Isotani, E., Olson, E.N., et al. (2002). Transcriptional co-activator PGC-1 alpha drives the formation of slow-twitch muscle fibres. Nature *418*, 797–801.

Luquet, S., Lopez-Soriano, J., Holst, D., Fredenrich, A., Melki, J., Rassoulzadegan, M., and Grimaldi, P.A. (2003). Peroxisome proliferator-activated receptor delta controls muscle development and oxidative capability. FASEB J. *17*, 2299–2301.

Ma, K., Chan, J.K., Zhu, G., and Wu, Z. (2005). Myocyte enhancer factor 2 acetylation by p300 enhances its DNA binding activity, transcriptional activity, and myogenic differentiation. Mol. Cell. Biol. *25*, 3575–3582.

McKinsey, T.A., Zhang, C.L., and Olson, E.N. (2001). Control of muscle development by dueling HATs and HDACs. Curr. Opin. Genet. Dev. *11*, 497–504.

McKinsey, T.A., Zhang, C.L., and Olson, E.N. (2002). MEF2: a calcium-dependent regulator of cell division, differentiation and death. Trends Biochem. Sci. *27*, 40–47.

Miniou, P., Tiziano, D., Frugier, T., Roblot, N., Le Meur, M., and Melki, J. (1999). Gene targeting restricted to mouse striated muscle lineage. Nucleic Acids Res. *27*, e27.

Narkar, V.A., Fan, W., Downes, M., Yu, R.T., Jonker, J.W., Alaynick, W.A., Banayo, E., Karunasiri, M.S., Lorca, S., and Evans, R.M. (2011). Exercise and PGC-1α-independent synchronization of type I muscle metabolism and vasculature by ERRγ. Cell Metab. *13*, 283–293.

Nebbioso, A., Manzo, F., Miceli, M., Conte, M., Manente, L., Baldi, A., De Luca, A., Rotili, D., Valente, S., Mai, A., et al. (2009). Selective class II HDAC inhibitors impair myogenesis by modulating the stability and activity of HDAC-MEF2 complexes. EMBO Rep. *10*, 776–782.

Nofsinger, R.R., Li, P., Hong, S.H., Jonker, J.W., Barish, G.D., Ying, H., Cheng, S.Y., Leblanc, M., Xu, W., Pei, L., et al. (2008). SMRT repression of nuclear receptors controls the adipogenic set point and metabolic homeostasis. Proc. Natl. Acad. Sci. USA *105*, 20021–20026.

Perissi, V., Jepsen, K., Glass, C.K., and Rosenfeld, M.G. (2010). Deconstructing repression: evolving models of co-repressor action. Nat. Rev. Genet. *11*, 109–123.

Picard, F., Kurtev, M., Chung, N., Topark-Ngarm, A., Senawong, T., Machado De Oliveira, R., Leid, M., McBurney, M.W., and Guarente, L. (2004). Sirt1 promotes fat mobilization in white adipocytes by repressing PPAR-gamma. Nature *429*, 771–776.

Pilegaard, H., Ordway, G.A., Saltin, B., and Neufer, P.D. (2000). Transcriptional regulation of gene expression in human skeletal muscle during recovery from exercise. Am. J. Physiol. Endocrinol. Metab. *279*, E806–E814.

Potthoff, M.J., and Olson, E.N. (2007). MEF2: a central regulator of diverse developmental programs. Development *134*, 4131–4140.

Rosenfeld, M.G., Lunyak, V.V., and Glass, C.K. (2006). Sensors and signals: a coactivator/corepressor/epigenetic code for integrating signal-dependent programs of transcriptional response. Genes Dev. *20*, 1405–1428.

Schiaffino, S., Gorza, L., Sartore, S., Saggin, L., Ausoni, S., Vianello, M., Gundersen, K., and Lømo, T. (1989). Three myosin heavy chain isoforms in type 2 skeletal muscle fibres. J. Muscle Res. Cell Motil. *10*, 197–205.

Sengupta, S., Peterson, T.R., Laplante, M., Oh, S., and Sabatini, D.M. (2010). mTORC1 controls fasting-induced ketogenesis and its modulation by ageing. Nature *468*, 1100–1104.

Smith, C.L., and O'Malley, B.W. (2004). Coregulator function: a key to understanding tissue specificity of selective receptor modulators. Endocr. Rev. *25*, 45–71.

Spiegelman, B.M., and Heinrich, R. (2004). Biological control through regulated transcriptional coactivators. Cell *119*, 157–167.

Storlien, L., Oakes, N.D., and Kelley, D.E. (2004). Metabolic flexibility. Proc. Nutr. Soc. *63*, 363–368.

Tanaka, T., Yamamoto, J., Iwasaki, S., Asaba, H., Hamura, H., Ikeda, Y., Watanabe, M., Magoori, K., Ioka, R.X., Tachibana, K., et al. (2003). Activation of peroxisome proliferator-activated receptor delta induces fatty acid beta-oxidation in skeletal muscle and attenuates metabolic syndrome. Proc. Natl. Acad. Sci. USA *100*, 15924–15929.

van Nas, A., Ingram-Drake, L., Sinsheimer, J.S., Wang, S.S., Schadt, E.E., Drake, T., and Lusis, A.J. (2010). Expression quantitative trait loci: replication, tissue- and sex-specificity in mice. Genetics *185*, 1059–1068.

Villena, J.A., and Kralli, A. (2008). ERRalpha: a metabolic function for the oldest orphan. Trends Endocrinol. Metab. *19*, 269–276.

Wang, Y.X., Zhang, C.L., Yu, R.T., Cho, H.K., Nelson, M.C., Bayuga-Ocampo, C.R., Ham, J., Kang, H., and Evans, R.M. (2004). Regulation of muscle fiber type and running endurance by PPARdelta. PLoS Biol. *2*, e294.

Watanabe, M., Houten, S.M., Mataki, C., Christoffolete, M.A., Kim, B.W., Sato, H., Messaddeq, N., Harney, J.W., Ezaki, O., Kodama, T., et al. (2006). Bile acids induce energy expenditure by promoting intracellular thyroid hormone activation. Nature *439*, 484–489.

Yu, C., Markan, K., Temple, K.A., Deplewski, D., Brady, M.J., and Cohen, R.N. (2005). The nuclear receptor corepressors NCoR and SMRT decrease peroxisome proliferator-activated receptor gamma transcriptional activity and repress 3T3-L1 adipogenesis. J. Biol. Chem. *280*, 13600–13605.

Zhang, C.L., McKinsey, T.A., Chang, S., Antos, C.L., Hill, J.A., and Olson, E.N. (2002). Class II histone deacetylases act as signal-responsive repressors of cardiac hypertrophy. Cell *110*, 479–488.

Zhang, Y., Ma, K., Sadana, P., Chowdhury, F., Gaillard, S., Wang, F., McDonnell, D.P., Unterman, T.G., Elam, M.B., and Park, E.A. (2006). Estrogen-related receptors stimulate pyruvate dehydrogenase kinase isoform 4 gene expression. J. Biol. Chem. *281*, 39897–39906.

Zhao, X., Sternsdorf, T., Bolger, T.A., Evans, R.M., and Yao, T.P. (2005). Regulation of MEF2 by histone deacetylase 4- and SIRT1 deacetylase-mediated lysine modifications. Mol. Cell. Biol. *25*, 8456–8464.